

The catalytic site structural gate of adenosine deaminase allosterically modulates ligand binding to adenosine receptors

Eduard Gracia,^{*,†,1} Daniel Farré,^{*,†,1} Antoni Cortés,^{*,†} Carles Ferrer-Costa,[‡] Modesto Orozco,^{†,‡} Josefa Mallol,^{*,†} Carme Lluís,^{*,†} Enric I. Canela,^{*,†} Peter J. McCormick,^{*,†} Rafael Franco,^{†,2} Francesca Fanelli,[§] and Vicent Casadó^{*,†,3}

*Laboratory of Molecular Neurobiology, Centro de Investigación Biomédica en Red sobre Enfermedades Neurodegenerativas (CIBERNED) and †Department of Biochemistry and Molecular Biology, Faculty of Biology, University of Barcelona, Barcelona, Spain; ‡Joint Institute for Research in Biomedicine–Barcelona Computing Center (IRB-BSC) Program on Computational Biology, Institute for Research in Biomedicine, §Dulbecco Telethon Institute and Department of Chemistry, Modena, Italy

ABSTRACT The enzyme adenosine deaminase (ADA) is a multifunctional protein that can both degrade adenosine and bind extracellularly to adenosine receptors, acting as an allosteric modulator regulating the hormonal effects of adenosine. The molecular regions of ADA responsible for the latter are unknown. In this work, alanine scanning mutagenesis of various ADA amino acid stretches, selected through *in silico* docking experiments, allowed us to identify regions of the enzyme responsible for modulating both its catalytic activity and its ability to modulate agonist binding to A₁ and A_{2A} adenosine receptors (A₁R and A_{2A}R). The combination of computational and *in vitro* experiments show that the structural gate to the catalytic site; *i.e.*, the α -1 helix containing residues L58-I72 and the loop containing residues A184-I188 of ADA, were important to maintain both the catalytic efficiency of the enzyme and its action as an allosteric modulator of the adenosine receptors. These data are consistent with a predicted supramolecular assembly, in which ADA bridges A_{2A}R and CD26 and are in line with the notion that the interaction of ADA with adenosine receptors has an important role in the immunosynapse. We propose that it is the ADA open form, but not the closed one, that is responsible for the func-

tional interaction with A₁R and A_{2A}R.—Gracia, E., Farré, D., Cortés, A., Ferrer-Costa, C., Orozco, M., Mallol, J., Lluís, C., Canela, E. I., McCormick, P. J., Franco, R., Fanelli, F., Casadó, V. The catalytic site structural gate of adenosine deaminase allosterically modulates ligand binding to adenosine receptors. *FASEB J.* 27, 000–000 (2013). www.fasebj.org

Key Words: multifunctional proteins • protein-protein interaction • enzyme mutants • *in silico* docking • immunological synapse

ADENOSINE DEAMINASE 1 (ADA; EC 3.5.4.4) is a key enzyme in the purine pathway catalyzing the irreversible deamination of adenosine or 2'-deoxyadenosine to inosine or 2'-deoxyinosine and ammonia (1). In humans, ADA is encoded by the 32-kb *Ada* gene on chromosome 20q (2) and occurs as a soluble 41-kDa monomer with 363 aa in all tissues. Inherited ADA deficiency is a rare metabolic disorder that causes lymphopenia and immunodeficiency due to toxic effects of its substrates. Most patients are infants with severe combined immunodeficiency disease (SCID) but healthy individuals with "partial" ADA deficiency have also been identified (3, 4). ADA deficiency accounts for ~15% of all SCID cases and one-third of autosomal recessive SCID cases. More than 70 ADA mutations, including >30 amino acid substitutions, have been found in patients (5 and references therein).

Abbreviations: A₁R, adenosine receptor A₁; A_{2A}R, adenosine receptor A_{2A}; A_{2B}R, adenosine receptor A_{2B}; ADA, adenosine deaminase; AR, adenosine receptor; CGS21680, 3-[4-[2-[[6-amino-9-[(2R,3R,4S,5S)-5-(ethylcarbamoyl)-3,4-dihydroxyoxolan-2-yl]purin-2-yl]amino]ethyl]phenyl]propanoic acid; EL, extracellular loop; GPCR, G-protein-coupled receptor; HDPR, 6-hydroxy-1,6-dihydropurine riboside; MD, molecular dynamics; NECA, *N*-ethyl-5'-carboxyamido-adenosine [(2S,3S,4R,5R)-5-(6-aminopurin-9-yl)-*N*-ethyl-3,4-dihydroxyoxolane-2-carboxamide]; ODA, optimal desolvation area; (R)-PIA, *N*6-(2-phenylisopropyl)-adenosine [(2R,3S,4R,5R)-2-(hydroxymethyl)-5-[[[(2S)-1-phenylpropan-2-yl]amino]purin-9-yl]oxolane-3,4-diol]; SCID, severe combined immunodeficiency disease; SDS-PAGE, sodium dodecyl sulfate-polyacrylamide gel electrophoresis

¹ These authors contributed equally to this work.

² Current address: Centro de Investigación Médica Aplicada, Universidad de Navarra, Pamplona, Spain.

³ Correspondence: Laboratory of Molecular Neurobiology, Department of Biochemistry and Molecular Biology, Faculty of Biology, University of Barcelona, Av. Diagonal 643, 08028 Barcelona, Spain. E-mail: vcasado@ub.edu
doi: 10.1096/fj.12-212621

This article includes supplemental data. Please visit <http://www.fasebj.org> to obtain this information.

Due to the release of ADA to the extracellular medium and the ability of the enzyme to bind to the cell surface, ADA is also expressed as an ectoenzyme with relevant physiological roles in medullary thymocytes, activated T cells, and epithelial cells (6–8). The first identified cell surface ADA binding protein was CD26/dipeptidyl peptidase IV (6, 7). CD26 is a multifunctional transmembrane glycoprotein that is widely expressed in most cell types, including epithelial cells and T lymphocytes, on which it is a marker of activation (9). The interaction between CD26 and ADA seems to be critical for the regulation of adenosine signaling in the immune system, for antigen presentation at the immunological synapse, and for the regulation of T-cell proliferation (8, 10, 11). CD26 also plays an important role in tumor biology (12–15) and together with ecto-ADA is selectively expressed on ALK-positive anaplastic large-cell lymphoma and Hodgkin's lymphoma (16). Using human-mouse ADA hybrids and ADA point mutants, Richard and coworkers (17, 18) localized the amino acids of ADA critical for CD26 binding into the α -helical segment P126-D143. Later, Weihofen and coworkers (19) crystallized the complex of the human CD26 ectodomain with bovine ADA. The crystal structure shows the existence of two intermolecular contacts that contribute to and stabilize the CD26-ADA complex formation. The first class of interactions is established between the loop A (I287-D297) of CD26 and the region successive to the α -1 helix (R76-A91) of ADA. The second class of intermolecular regions are between the loop B (D331-Q344) of CD26 and α -2 helix (P126-D143) of ADA, the same α -helix previously reported by Richard and coworkers (17, 18) from mutagenic studies (see above).

The second type of ecto-ADA-binding proteins includes the adenosine receptors (ARs) A_1 (A_{1R} ; refs. 20–23), A_{2A} (A_{2AR} ; ref. 24), and A_{2B} (A_{2BR} ; ref. 25), which are members of the rhodopsin family of G-protein-coupled receptors (GPCRs). Binding of enzymatically active or Hg^{2+} -inactivated ADA to A_{2BR} increases the receptor affinity and signaling through protein-protein interactions (25). The ADA- A_{1R} interaction is important because the enzyme potentiates signal transduction and modulates A_{1R} desensitization (20, 26). Very recently, we have shown that ADA binds to human A_{1R} and A_{2AR} , behaving as an allosteric effector that markedly enhances agonist affinity and increases receptor functionality (21, 24). The physiological role of the ADA-AR interactions is to make these receptors more sensitive to adenosine (21, 24). Besides these binary ADA-AR complexes, higher-order protein complexes containing both ADA and ARs have been postulated. We hypothesized the existence of functional heteromeric ADA- A_{1R} -dopamine D_1 receptor complexes in cortical neurons and proposed that their formation can be modulated by both dopamine and adenosine (27). In addition, we have shown that ADA anchored to the dendritic cell surfaces, most likely by the A_{2BR} , binds to CD26 expressed on the surface of the T cells (8). In this case, it has been postulated that ADA acts as a bridge

between dendritic cells and lymphocytes in the immunosynapse triggering costimulation. This costimulatory signal promotes an augmented T-cell activation with a T-helper 1 pattern and proinflammatory cytokine production, therefore enabling an enhanced immune response (28, 29).

Although the intermolecular contacts that contribute to and stabilize the CD26-ADA complex formation are known, the ADA portions involved in the interaction with ARs have not been studied. The aim of the present study was to characterize the regions of ADA involved in the interaction with ARs. For this purpose, we subjected to alanine scanning mutagenesis a number of ADA amino acid stretches predicted by docking experiments as likely involved in interaction with the A_{2AR} . The effects of the mutations on the catalytic efficiency of ADA and on the ADA-induced increase in agonist binding to A_{1R} and A_{2AR} led to predict the ADA amino acid stretches L58-I72 and A183-I188 as involved in AR recognition.

MATERIALS AND METHODS

Computational analysis

Docking simulations

We performed docking simulations between ADA and the A_{2AR} . Predictions of likely interfaces between ADA and the extracellular portions of the A_{2AR} , which drove *in vitro* alanine scanning mutagenesis done in this study, were carried out before the release of the first crystal structure of the A_{2AR} . The ZDOCK program was used (30). Since the original idea was to investigate whether a likely homodimeric architecture of the A_{2AR} could interact with both protomers in the crystallographic dimeric complex between ADA and CD26, we first predicted an A_{2AR} homodimer by using a computational model of the protomer (31). Quaternary structure predictions followed an established computational protocol (32–36). The predicted dimer, characterized by H4-H5 and I2-I2 contacts, was then employed as a fixed protein (*i.e.*, target), whereas ADA was employed as a mobile protein (*i.e.*, probe). As for the latter, both the H and G chains extracted from the dimeric complex with CD26 [Protein Data Bank (PDB) code 1W1I; ref. 19] were used. To improve sampling, the docking search excluded the transmembrane and cytosolic portions of the A_{2AR} (*i.e.*, 8–66, 79–138, 177–253, and 271–412) as well as the ADA portions interacting with CD26 (*i.e.*, 24–32, 74–94, and 124–145). A rotational sampling interval of 6° was employed, and the best 4000 solutions were retained and subjected to cluster analysis by using a C_α -root mean square deviation (RMSD) of 4.0 Å as a threshold. The latter was based on the QT clustering algorithm (37). Cluster centers were subjected to visual inspection. Only one docking pose was characterized by a simultaneous and symmetric interaction between the two A_{2AR} protomers in the dimer and the two ADA monomers. Only one docking pose turned out to be reliable and characterized by a simultaneous and symmetric interaction between the two A_{2AR} protomers in the dimer and two ADA protomers. This docking pose was shared by 3 low-populated clusters; *i.e.*, each made of 7, 5, and 4 solutions. The highest-scored solution belonged to the 7-solution cluster and was the 225th best-scored one out of 4000. In this complex, the following amino acid stretches from

ADA; *i.e.*, 58–66, 114–118, 155–158, and 184–188, were found to participate in the ADA-A_{2A}R interface. Those stretches were subjected to the *in vitro* alanine scanning mutagenesis shown in this study, which highlighted the 58–66 and 184–188 portions as playing a role in A_{2A}R recognition (see below). The current availability of a number of crystal structures of the human A_{2A}R imposed us to repeat the docking simulations to improve the resolution level of the prediction. Indeed, mayor differences in the extracellular portions between rhodopsin-based model and crystal structure reside in extracellular portion 2 (E2), which is significantly more exposed to the solvent in the crystal structure than in the model (results not shown). Therefore, the crystal structures of the human A_{2A}R in complex with the adenosine and (2*S*,3*S*,4*R*,5*R*)-5-(6-aminopurin-9-yl)-*N*-ethyl-3,4-dihydroxyoxolane-2-carboxamide [*N*-ethyl-5'-carboxyamido-adenosine (NECA)] agonists (PDB code 2YDO and 2YDV, respectively; ref. 38) holding the complete 3 extracellular loops (ELs) were employed as targets. As for ADA, the 1WII:G chain, as well as the structures of isolated ADA in complex with the 6-hydroxy-1,6-dihydropurine riboside (HDPR) transition-state analog (PDB code 1KRM; ref. 39) and of the unbound form (PDB code 1VFL; ref. 40) were employed as probes. The 3 ADA structures differ for the conformation and orientation of the 58–69 helix, which is closer to the 184–188 loop in 1KRM (closed form) than in the 1VFL structure (open form). Such amino acid stretches had indeed been predicted as participating in the ADA-A_{2A}R interface by early docking experiments and validated by *in vitro* alanine scanning mutagenesis (see below). We did not consider the 1WXY structure, since it is quite similar to 1VFL. The 1WII:G structure is, instead, between 1KRM and 1VFL, closer to the latter. To minimize indeterminations in the structural models of the target and probe proteins, both ADA and A_{2A}R were considered in their monomeric forms. Docking simulations and cluster analysis of the best 4000 docking solutions followed the same protocol described above. The centers of the most populated clusters were finally subjected to visual analysis.

Molecular dynamics (MD) simulations

MD simulations were carried out on the 1VFL and 1WXY structures of ADA, selected based on sequence completeness and resolution. These structures are very related, but 1VFL is bound to Zn ion, and 1WXY is additionally bound to the Fr104783 ligand. These two structures were used to generate starting models for MD simulations in both holo and apo forms (obtained by removing ligands). For this purpose, the monomeric crystal structure was fully solvated with an octahedron tip3p water box; ions were added, and final system was minimized and equilibrated to 300 K using amber force field (41) and implemented in the NAMD program (42, 43). Finally, 100 ns of production were collected in the isothermic-isobaric ($P=1$ atm, $T=298$ K). Particle mesh Ewald (44) was used to account for long-range electrostatic effects. RESPA (45) algorithm with a minimum integration step of 1 fs was used, keeping all bonds connecting hydrogens constrained using the RATTLE algorithm (46). Additional technical details on simulation setup, curation, and analysis are identical to those described elsewhere (47). Results from 4 dynamics are similar, and we observed a fluctuation from a “closed” state to an “open” one due to the movement of a helix, increasing solvent accessibility to the protein. All four dynamics show a normal behavior based on geometrical and energetic results. Typical trajectories are available in the MoDEL database (ref. 48; <http://mmb.pcb.ub.es/MoDEL/>). Optimal desolvation area calculations were performed on the collected trajectories defining the optimal patches from the center of coordinates of every residue side chain (49, 50).

Bacterial strains and vector

Escherichia coli SΦ 3834, a multiple auxotroph (*rpsL*, *Dadduid-man*, *metB*, *guaA*, *uraA:Tn 10*) with a deletion of add (bacterial ADA gene), and plasmid pZC11-containing TAC-promoted wild-type human ADA cDNA (51) were used. Overnight cultures of pZC11-hADA transformants of SΦ 3834 were inoculated into the appropriate volume of Luria-Bertani (LB) medium supplemented with carbenicillin and tetracycline (200 and 18.75 μg/ml, respectively) (Sigma-Aldrich, Madrid, Spain). Cells were grown with shaking at 37°C until an A₆₀₀ nm = 1.0 and then were harvested and frozen at –80°C (18).

Site-directed mutagenesis

Site-directed mutagenesis was performed on the human ADA *wt* gene cloned into the pZC11 vector as described in the QuickChange Site-Directed Mutagenesis Kit protocol (Stratagene, La Jolla, CA, USA). Oligonucleotides were designed according to the guidelines described in the Stratagene protocol. One, 2, or 3 nucleotides, depending on the nucleotide sequence, were changed in order to obtain the desired mutation (Table 1). Polymerase chain reactions were carried out with 0.3 μM of each mutagenic primer (Sigma-Aldrich), 0.2 mM of each dNTP (Promega, Madison, WI, USA), 50–100 ng of the template, 1 μl of 2.5 U/μl of PfuTurbo DNA polymerase (Stratagene), and 5 μl of 10× reaction buffer (200 mM Tris-HCl, pH 8.8; 20 mM MgSO₄; 100 mM KCl; 100 mM (NH₄)₂SO₄; 1% Triton X-100; and 1 mg/ml nuclease-free bovine serum albumin) in a final volume of 50 μl. The samples were subjected to 12 cycles of amplification with denaturation at 95°C for 30 s, annealing at 55°C for 1 min, and extension at 72°C for 5 min using an iCycler thermal cycler (Bio-Rad Laboratories, Hercules, CA, USA). Then, the reaction was cooled to 37°C and incubated for 1 h with 2 μl (10 U/μl) of *Dpn* I (Promega) at 37°C. The reaction product was transformed into *E. coli* SΦ 3834 and grown overnight with the appropriate antibiotic, and colonies were checked in order to determine that only the desired mutation was present.

Partial purification of ADA

Recombinant wild-type and ADA mutants were partially purified from 4-L cultures of *E. coli* SΦ 3834 cells, transformed with the plasmid pZC11 containing the cDNA of ADA. Unless otherwise indicated, all steps were carried out at 4°C. Cell pellets were resuspended in 40 ml of lysis buffer [10 mM Tris-HCl, pH 7.5; 75 mM KCl; 10 mM MgCl₂; 1 mM dithiothreitol; and a protease inhibitor cocktail (Sigma-Aldrich) containing 4-(2-aminoethyl) benzenesulfonyl fluoridehydrochloride to a final concentration of 1 mM]. The suspension was distributed into 20-ml batches, cooled on ice, and sonicated for 24 × 20 s in a Branson digital sonifier (Branson Ultrasonics Corp., Danbury, CT, USA) at 15% intensity. The resulting homogenate was centrifuged at 105,000 *g* for 60 min, and protamine sulfate (Sigma-Aldrich) was slowly added to the clarified extract up to a final concentration of 2 mg/ml. After 60 min of constant stirring, the suspension was centrifuged as before, and the supernatant was dialyzed twice (~12 h) with continuous stirring against a 50× excess volume of 20 mM Tris-HCl buffer (pH 7.4) containing 1 mM dithiothreitol and 3 mg/ml of activated charcoal (Sigma-Aldrich). The dialysate was applied (flow rate 20 ml/h) to a Q Sepharose HP (GE Healthcare Europe, Cerdanyola, Spain) anion exchanger column (5×5 cm) preequilibrated with 20 mM Tris-HCl buffer (pH 7.4) and 1 mM dithiothreitol. The

TABLE 1. Mutagenic oligonucleotide primers

Mutation	Primer	Codon position	Sequence
L58A	Forward Reverse	172–174	5'-GACAAGCCGCTCACC _g cGCCAGACTTCCTG-3' 5'-CAGGAAGTCTGGC _g cGGTGAGCGGCTTGTC-3'
D60A	Forward Reverse	178–180	5'-CCGCTCACCTTCCA _g cCTTCTCGGCCAAG-3' 5'-CTTGGACAGGAAGG _c TTGGAAGGGTGAGCGG-3'
F61A	Forward Reverse	181–183	5'-CTCAACCTTCCAGAC _g cTCTGGCCAAGTTT-3' 5'-AAACTTGGCCAGA _g cGTCTGGAAGGGTGAG-3'
L62A	Forward Reverse	184–186	5'-ACCCTTCCAGACTT _g cGGCCAAAGTTTGAC-3' 5'-GTCAAACCTTGGCCC _g cAAGTCTGGAAGGGT-3'
K64A	Forward Reverse	190–192	5'-CAGACTTCTGGCC _g cATTTGACTACTACATGC-3' 5'-GCATGTAGTAGTCAAAT _g cGGCCAGGAAGTCTG-3'
F65A	Forward Reverse	193–195	5'-CCTGGCCAAG _g cTGACTACTACATGCC-3' 5'-GGCATGTAGTAGTCA _g cCTTGGCCAGG-3'
D66A	Forward Reverse	196–198	5'-CCTGGCCAAGTTT _g cTTACTACATGCCTGC-3' 5'-GCAGGCATGTAGTAA _g cAAACTTGGCCAGG-3'
M69A	Forward Reverse	205–207	5'-GTTTACTACTACG _g cGCTGCTATCGCGGGCTG-3' 5'-CAGCCCGGATAGCAGC _g cCGTAGTAGTCAAAC-3'
I115A	Forward Reverse	343–345	5'-CCAAAGTGGAGCCA _g cTCCTTGGAAACCAGCG-3' 5'-GCCTGGTTCCAGGGA _g cTGGCTCCACTTTGG-3'
N118A	Forward Reverse	352–354	5'-GCCAATCCCCTGG _g cCCAGGCTGAAGG-3' 5'-CCTTCAGCCTGG _g cCCAGGGGATTGGC-3'
M155A	Forward Reverse	463–465	5'-TCCATCCTGTGCTGC _g cGGCCACCAGCCC-3' 5'-GGGCTGTTGGCGC _g cGCAGCACAGGATGGA-3'
H157A	Forward Reverse	469–471	5'-GCTGCATGGCG _g cTCAGCCCAACTGG-3' 5'-CCAGTTGGGCTGA _g cGCCATGCAGC-3'
G184Q	Forward Reverse	550–552	5'-CGATCCTGGCTc _g AGATGAGACCATCC-3' 5'-GGATGGTCTCATC _c t _g AGCCAGGATCG-3'
D185A	Forward Reverse	553–555	5'-CCTGGCTGGAG _c TGAGACCATCCC-3' 5'-GGGATGGTCTCA _g cTCCAGCCAGG-3'
L194A	Forward Reverse	580–582	5'-GCAGCCTC _g cGCCCTGGACATGTCC-3' 5'-GGACATGTCCAGGGC _g cGAGGCTGC-3'

Sequence mismatches are indicated in lowercase letters.

column was washed (20 ml/h) with 2 vol of equilibration buffer, and thereafter the enzyme was eluted (5-ml fractions) with 100 ml of a linear NaCl gradient (0–0.25 M) in the equilibration buffer. ADA active fractions were always recovered in the same fractions with a similar yield (60–70%). Eluates with highest ADA content were pooled, desalted with a PD10 (GE Healthcare) gel filtration column, preequilibrated with 50 mM, pH 7.4, Tris-HCl buffer, and stored at 4°C for their immediate use within the next 24 h. The amount of ADA in these samples was evaluated by immunoblotting, using a standard curve obtained with known amounts of pure wild-type human ADA, purified by the method of Gracia *et al.* (21), performed as internal control in each experiment.

Enzyme activity and ADA inhibition

Unless otherwise indicated, enzyme activity was determined at 25°C with 0.1 mM adenosine as substrate in 50 mM Tris-HCl buffer, pH 7.4. The decrease in the absorbance at 265 nm ($\Delta\epsilon=7800 \text{ M}^{-1} \text{ cm}^{-1}$) was monitored in an Ultrospec 3300 pro spectrophotometer (Biochrom Ltd., Cambridge, UK); 1-ml cuvettes with a 1-cm light path length were used. One unit (U) of ADA activity is defined as the amount of enzyme required to hydrolyze 1 μmol of adenosine per minute in the conditions of the assay. Hg^{2+} or deoxycoformycin inactivation of wild-type ADA was performed by a preincubation (2 h for Hg^{2+} or 30 min for deoxycoformycin) of 15 U/ml of desalted ADA with 100 μM HgCl_2 or 10 nM deoxycoformycin, and removal of free inhibitor by two consecutive gel filtrations, as described previously (22). No residual activity was found after adding a high excess (8 $\mu\text{g}/\text{ml}$) of inhibited

enzyme to 0.1 mM adenosine for 4 h in the conditions described above or when the activity was determined after 2 h incubation of the enzyme in the buffer used to obtain the enzyme or in the buffer used for ligand binding (Supplemental Table S1). To check that Hg^{2+} -treated ADA remains inactive during binding assays, we performed a competition curve of the A_1R agonist [^3H] (2*R*,3*S*,4*R*,5*R*)-2-(hydroxymethyl)-5-[6-[[2*S*]-1-phenylpropan-2-yl]amino]purin-9-yl]oxolane-3,4-diol {N6-(2-phenylisopropyl)-adenosine [(R)-PIA]} binding *vs.* increasing adenosine concentrations in the presence of untreated ADA or in the presence of Hg^{2+} -inhibited ADA (Supplemental Fig. S1). In the presence of untreated ADA the [^3H] (R)-PIA binding was unchanged according to the degradation of the competing adenosine by the active ADA. In contrast, in the presence of Hg^{2+} -inhibited ADA, we obtained a competition curve in which the [^3H] (R)-PIA binding diminished when increasing adenosine concentration, according to the lack of enzymatic activity of Hg^{2+} -inhibited ADA.

Kinetic parameters

Steady-state kinetic measurements were performed in 50 mM Tris-HCl buffer (pH 7.4) using a series of 6 concentrations of adenosine (ranging from 10 μM to 1 mM) and a constant enzyme concentration for which the initial steady-state velocities were measured with <10% substrate depletion for the first 30–120 s of the reaction. Inhibition studies were carried out by monitoring the hydrolysis rates of adenosine, as outlined before, in the presence of 3 increasing constant concentrations of purine riboside (ranging from 5 μM to 0.5

mM; Sigma-Aldrich). In all cases, a minimum of 4 replicates for each single experimental point were performed. Kinetic parameters were obtained by fitting the experimental data to the appropriate rate equations by nonlinear regression, using the commercial Grafit curve-fitting software (Erithacus Software, Surrey, UK). Parameters are expressed as values \pm SE.

Protein determination

Protein was quantified by the bicinchoninic acid (Pierce Chemical Co., Rockford, IL, USA) method (52) using bovine serum albumin dilutions as standard.

Electrophoresis and immunoblotting

Sodium dodecyl sulfate–polyacrylamide gel electrophoresis (SDS-PAGE) was carried out using homogeneous slab gels (12% acrylamide running gel and 4% stacking gel) that were electrophoresed at 35 mA/gel constant current for 90 min in a miniprotean system (Bio-Rad Laboratories SA, Barcelona, Spain). The Rainbow molecular weight markers (GE Healthcare) were used as standards, and proteins were visualized by staining with Coomassie Brilliant Blue (Sigma-Aldrich). For immunoblotting, proteins separated by SDS-PAGE were transferred to Hybond-P polyvinylidene difluoride membranes (GE Healthcare), using wet Bio-Rad Trans-Blot equipment. Membranes were consecutively incubated with 2.5 μ g/ml rabbit anti-human ADA and horseradish peroxidase-conjugated goat anti-rabbit IgG (Pierce), diluted 1:40,000, as primary and secondary antibodies, respectively. After washing, they were subsequently incubated with chemiluminescence detection solutions (SuperSignal West Pico Chemiluminescent Substrate; Pierce). Band images were obtained using an image analyzer (LAS-3000; Fuji Film, Tokyo, Japan) and quantified using the Multi Gauge V3.0 software (Fuji Film).

Brain striatal membrane preparations and radioligand binding experiments

As a source of A₁R and A_{2A}R, we used sheep brain striatal membranes, since we previously determined that human ADA produces similar effects on human and sheep A₁R and A_{2A}R (ref. 21 and results not shown). Membrane suspensions from sheep brain striatum were prepared as described previously (53). Tissue was disrupted with a Polytron homogenizer (PTA 20 TS rotor, setting 3; Kinematica, Basel, Switzerland) for three 5-s periods in 10 vol of 50 mM Tris-HCl buffer (pH 7.4) containing a protease inhibitor cocktail (1:1000; Sigma-Aldrich). Membranes were then obtained by centrifugation at 105,000 *g* (40 min, 4°C), after eliminating cell debris by centrifugation (1000 *g*, 10 min, 4°C), and the pellet was homogenized and centrifuged under the same conditions. Membranes were stored at –80°C and were washed once more as described above and homogenized in 50 mM Tris-HCl buffer for immediate use.

ADA dose-dependent curves were obtained by incubating (2 h) striatal membrane suspensions (0.3 mg of protein/ml) with A₁R agonist [³H] (R)-PIA (0.5 nM, 30 Ci/mmol; Moravek Biochemicals Inc., Brea, CA, USA) or A_{2A}R agonist [³H] 3-[4-[2-[[6-amino-9-[(2*R*,3*R*,4*S*,5*S*)-5-(ethylcarbamoyl)-3,4-dihydroxy-oxolan-2-yl]purin-2-yl]amino]ethyl]phenyl]propanoic acid (CGS21680; 20 nM, 42.7 Ci/mmol; Perkin Elmer, Boston, MA, USA) in the absence or in the presence of the indicated amounts of the wild-type or mutant ADA at 25°C in 50 mM Tris-HCl buffer (pH 7.4) containing 10 mM MgCl₂. In all cases, free and membrane-bound radioligand were separated by rapid filtration of 500- μ l aliquots in a cell harvester (Brandel,

Gaithersburg, MD, USA) through Whatman GF/C filters embedded in 0.3% polyethylenimine (Sigma-Aldrich), which were subsequently washed for 5 s with 5 ml of ice-cold Tris-HCl buffer. The filters were incubated with 10 ml of Ecoscint H scintillation cocktail (National Diagnostics, Atlanta, GA, USA) overnight at 23°C, and radioactivity counts were determined using a Tri-Carb 1600 scintillation counter (Perkin Elmer Life and Analytical Sciences, Downers Grove, IL, USA) with an efficiency of 62% (53). Nonspecific binding was defined as the binding remaining in the presence of 10 μ M (R)-PIA or 10 μ M CGS21680 (Sigma-Aldrich).

RESULTS

Prediction of likely interfaces between ADA and A_{2A}R

Docking simulations between ADA and the human A_{2A}R, which served to drive the *in vitro* experiments, were carried out when no high-resolution structure of the A_{2A}R was available (see Materials and Methods). Such simulations highlighted the contribution of the 58–66, 114–118, 155–158, and 184–188 portions of ADA to the ADA-A_{2A}R interface. The crystal structures of the agonist-bound forms of A_{2A}R characterized by a complete determination of the extracellular portions were released in May 2011 (38). Therefore, in order to improve the accuracy of the predicted ADA-A_{2A}R interface, we have redone docking experiments by using both the crystal structures of the adenosine- and NECA-bound forms of the A_{2A}R (PDB codes 2YDO and 2YDV, respectively). Only the results of such experiments are shown. Since it has been observed that ADA has two distinct conformations, named the open form and the closed forms (40, 54–56), in which the structural gate of the active site pocket (the α helix, T57–A73, and the peptide backbone of a β strand, L182–D185) have different conformations, three different crystal structures of the ADA protomer were probed. These structures differ in the opening of the structural gate to the catalytic pocket; *i.e.*, in the distance between the amino acid stretches L58–I72 and A184–I188. The best 4000 solutions from docking simulations between the 1YDV A_{2A}R structure and the 1WII:G ADA structure were divided into 341 clusters, 48 of which made \geq 20 solutions and covered 32% of the total docking poses. Selection of the likely interface was based on a docking score, cluster population, reliability of the complex in the context of the membrane topology of the A_{2A}R, and minimization of bad contacts. Indeed, the selected docking pose was the top hit solution, *i.e.*, solution 1; it fell in the second most populated cluster (made of 62 solutions), and, in line with the results of early docking simulations, it was characterized by a central role for the amino acid stretches 54–67 and 184–189 (Fig. 1A, violet and orange stretches, respectively) in recognizing the extracellular portions of the A_{2A}R. In detail, the 55–65 helix (Fig. 1A, violet) interacts with the receptor EL2, whereas the 184–189 stretch (Fig. 1A, orange) interacts with the N terminus of the receptor. Salt bridge interactions can form between D60 of ADA and

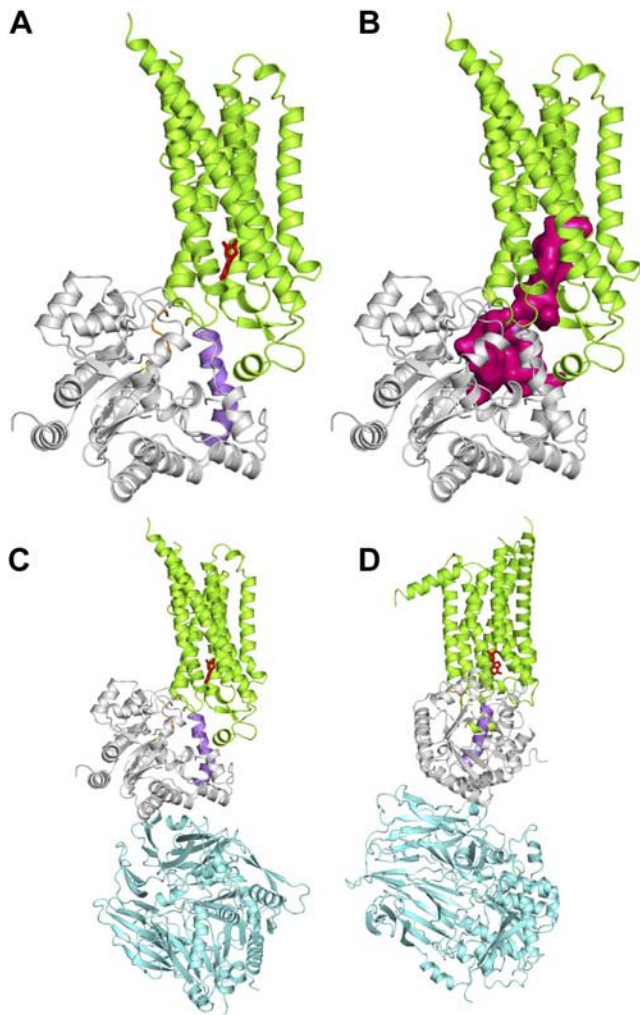


Figure 1. Predicted complex between ADA and A_{2A}R. *A*) Cartoons of A_{2A}R (lemon-green) in complex with ADA (gray). Such a complex is solution 1 of 4000 docking solutions (*i.e.*, the best one). A_{2A}R is shown in a direction parallel to the membrane surface, with the intracellular side on top. ADA amino acid stretches 58–72 and 183–188 interacting with the receptor are shown in violet and orange, respectively. Adenosine is represented as red sticks. *B*) Same view as in *A*; the channel connecting the adenosine binding site in A_{2A}R with the catalytic site of ADA is highlighted in magenta. Such a crevice was computed by the AutoDock tool AutoLigand (63). *C, D*) Two views of the quaternary complexes between adenosine-bound A_{2A}R (lemon-green), ADA (gray), and CD26 (cyan). Adenosine agonist is represented as red sticks.

both K150 and K153 of the A_{2A}R, as well as between D185 of ADA and the positively charged N terminus of the A_{2A}R. Other interactions include K54^{ADA}-D261^{A_{2A}R}, D66^{ADA}-H155^{A_{2A}R}, and D118^{ADA}-H155^{A_{2A}R}. It is worth noting that a channel connects the adenosine binding site in the A_{2A}R and the catalytic pocket of ADA (Fig. 1*B*). Remarkably, the predicted ADA-A_{2A}R docking mode is such that ADA can make a complex, in which ADA acts as a bridge between A_{2A}R and CD26 (Fig. 1*C, D*). For the docking between A_{2A}R and the 1VFL (unbound open form) and 1KRM (HDPR-bound structure, closed form) structures, in both cases, docking solutions similar to the predicted one could be found,

though lower docking scores were found for the closed form.

Mapping potential protein-protein interaction sites on different conformational states of ADA

We investigated the intrinsic flexibility of ADA by MD simulations. MD simulations were carried out on the 1VFL and 1WXY structures of ADA. Analysis of 4 MD runs clearly yielded 2 states of the enzyme, one in an open form and the other in a closed form (see Supplemental Figs. S2–S7). Supplemental Figs. S3 and S6 show the RMS of the backbone during the trajectory after minimization for both 1VFL and 1WXY ADA structures. Fluctuation of structures below 2 Å is expected for proteins at that size of runs (10 ns). Supplemental Figs. S4 and S7 show the evolution of solvent accessible area during the dynamics for both 1VFL and 1WXY ADA structures. No changes are observed, as expected, and solvent accessible area is almost constant. The main difference between these two states is a change in the conformation of an α helix (residues 58–72) and a loop (residues 182–185) on the catalytic site of the enzyme (see Supplemental Figs. S2 and S5). In the open state, these regions are in a more relaxed conformation, allowing the ligand to enter and leave the catalytic site. In the closed state, the conformation is more rigid and does not allow movement of adenosine. These conformational states correspond to the ADA open and closed forms detected previously (40, 54–56). The 1KRM crystallographic structure (a claimed closed form) is more similar to the closed form obtained by MD (RMSD=1.1 Å) than to the open form obtained by MD (RMSD = 1.9 Å) and the type of open ↔ closed transition is exactly the one found in MD simulations, giving support to these conformational states corresponding to the ADA open and closed forms detected previously. However, it is important to note that the 1KRM structure shows a stronger packing of the helix than that found even for the closed state in our MD simulations (Supplemental Fig. S8). Optimal desolvation area (ODA) is one of the driving forces for protein-protein interactions, therefore ODA calculations were used to map potential interaction sites on the surface of ADA. We followed patches of ODA during the entire simulation period for the open and closed states. In line with predictions of docking experiments, a combination of data coming from ODA calculations, distance measurements, and binding energy determinations highlighted the L58-Y67 and A183-D185 ADA stretches as potentially involved in protein-protein interactions.

Mutagenesis, expression, and partial purification of ADA mutants

We have chosen representative ADA mutations that cover the different putative amino acid stretches involved in the interaction of ADA with the AR deduced from docking studies. The ADA mutants included

alanine substitutions for L58, D60, F61, L62, K64, F65, D66, M69, I115, N118, M155, H157, D185, L194, and glutamine substitution for G184. The mutated positions in the primary and secondary structure of ADA are shown in **Fig. 2**. ADA mutations were generated by site-directed mutagenesis directly into the pZC11 plasmid containing the human ADA cDNA, as described in Materials and Methods, using the mutagenic oligonucleotide primers described in Table 1. Mutants were expressed in an ADA-deficient *E. coli* strain, *E. coli* SΦ 3834, under standardized conditions. To check the ADA expression, immunoblot bands for the enzyme were quantified in supernatants of sonicated ADA-expressing *E. coli* SΦ 3834 extracts (see Materials and Methods). As assessed by immunoblotting, ADA mutants were usually well expressed, ranging from 29 to 141% of the value obtained with the wild-type enzyme, 80 μg/ml (**Fig. 3**; see Supplemental Fig. S9 for the whole Western blotting images).

To investigate the ADA epitopes involved in the interaction with ARs, partially purified preparations of the wild-type and mutant enzymes were used. The purification protocol includes a protamine sulfate treatment to remove nucleic acids and an anionic-exchange chromatography through Q-Sepharose, as detailed in Materials and Methods. In all cases, the enzyme was recovered in the same fractions with a similar yield (60–70%). However, the specific activity of several ADA mutants was clearly different from the value corresponding to the wild-type enzyme (**Table 2**). This fact strongly suggests the existence of changes in the catalytic efficiency of ADA due to modifications in the kinetic parameters of the enzyme.

Steady-state kinetic parameters for the wild-type and mutant enzymes

To examine the effect of mutations on the catalytic behavior of ADA, the kinetic parameters of the purified wild-type and ADA mutants were determined using

adenosine as substrate. The values of K_m , k_{cat} , and catalytic efficiency (k_{cat}/K_m), for the recombinant enzyme and for the different mutants were determined. In addition, to further probe the extent of the conservation of the active site pocket structure, the affinity constant for a ground-state inhibitor, purine riboside [$K_{i(PR)}$], acting as a competitive inhibitor of the enzyme with respect to the adenosine, was also determined. The kinetic data are summarized in **Table 3**. For D66, I115, and L194 mutants, very similar parameters, compared to the wild-type enzyme, were obtained and, only moderate differences in some of the kinetic parameters were detected for the D60, K64, N118, H157, G184, and D185 mutants. Mutations in F61, F65, M69, and M155 cause a decrease of one order of magnitude in the catalytic efficiency. For F61 or M69 mutated enzymes, the decrease in the catalytic efficiency was due to a decrease in k_{cat} but not in K_m values, indicating that the mutations are important to reach V_{max} . For M155 or F65 mutated enzymes, both k_{cat} and K_m values were altered, indicating that both V_{max} and the affinity for the substrate were decreased. Finally, the major alterations in the k_{cat} and the K_m were detected for L58 and L62 mutants, resulting in a decrease of two orders of magnitude on their catalytic efficiency. For these mutants, changes detected on both the k_{cat} and K_m values indicate that both the substrate affinity and the maximum velocity were decreased, suggesting that these mutations alter the structure of the catalytic pocket. This was corroborated by the 70-fold higher $K_{i(PR)}$ value obtained for these mutants compared to the wild-type enzyme.

Effect of ADA mutations on the agonist binding to A₁R and A_{2A}R

To investigate whether the mutated amino acids on the ADA molecule are involved in the interaction with the ARs, we compared the agonist binding to A₁R and A_{2A}R in the absence of ADA, in the presence of wild-type

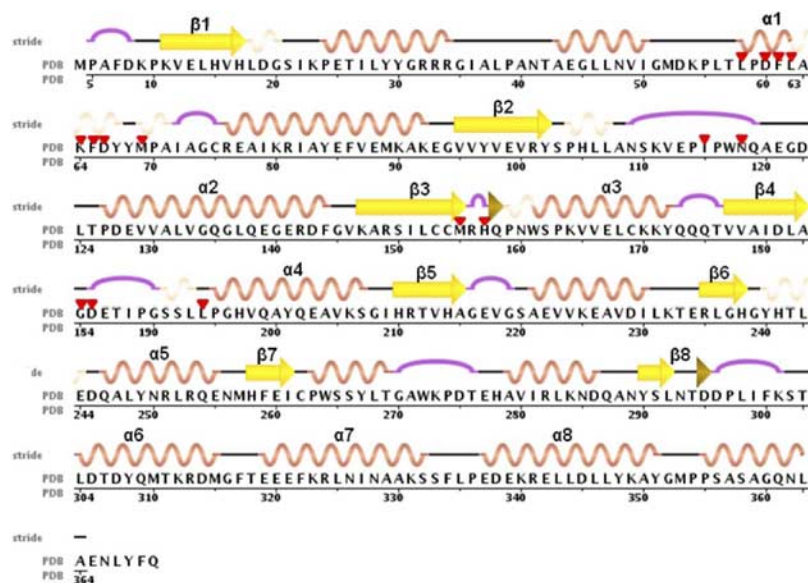


Figure 2. Primary and secondary structure of human ADA. Point mutations generated by site-directed mutagenesis are shown with red triangles. Primary α helices are shown in pink, β strands are in yellow, hydrogen-bonded turns are in purple, and isolated residues forming β bridges are in brown. Image generated with the algorithm developed by Frishman and Argos (64).

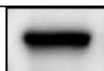


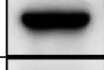








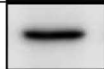


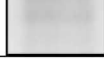
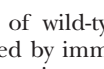
Enzyme	Immunoblotting	[ADA] (Q-Sepharose) ($\mu\text{g/ml}$)
Wild type		80 \pm 10
L58A		113 \pm 5
D60A		50 \pm 10
F61A		80 \pm 10
L62A		60 \pm 10
K64A		60 \pm 6
F65A		62 \pm 2
D66A		78 \pm 7
M69A		50 \pm 10
I115A		37 \pm 6
N118A		80 \pm 10
M155A		23 \pm 3
H157A		70 \pm 10
G184Q		32 \pm 5
D185A		34 \pm 3
L194A		100 \pm 10
S Φ 3834		0

Figure 3. Expression of wild-type and mutant ADA. ADA expression was detected by immunoblotting, as described in Materials and Methods, using supernatants of sonicated ADA-expressing *E. coli* S Φ 3834 extracts. Quantification of the immunoblot band was done by interpolation in a standard curve obtained by immunoblotting known amounts of pure human ADA as an internal control in each experiment (see Materials and Methods). Values are means \pm SE of 3 independent experiments.

ADA, or in the presence of mutated ADA. We performed these experiments with increasing concentrations of ADA to determine, from the dose-response curves, the amount of the enzyme able to produce the 50% of the maximum agonist binding increases (EC_{50} values). This is a parameter related to the enzyme affinity for the receptors. We also determined the ADA-induced maximum effect, *i.e.*, the effect on ligand binding produced by the highest ADA concentration.

ADA dose-response curves were obtained by incubating (2 h) brain membrane suspensions (0.3 mg of protein/ml) with 0.5 nM [^3H] (R)-PIA or 20 nM [^3H]CGS21680 in the presence or in the absence of increasing amounts of the wild-type or mutant ADA (0.1 $\mu\text{g/ml}$ to 100 $\mu\text{g/ml}$) at 25°C in 50 mM Tris-HCl buffer (pH 7.4) containing 10 mM MgCl_2 , as described in Materials and Methods. Wild-type ADA dose-responsively enhanced (R)-PIA binding to striatal $A_1\text{R}$ (Fig. 4A, black curve) and CGS21680 binding to striatal $A_{2A}\text{R}$ (Fig. 4C, black curve), with EC_{50} values of 8 and 7 ng/ml, respectively, and with a maximum ligand binding increase of $\sim 85\%$ with respect to the ligand binding in the absence of ADA (Table 4). According to our previous results (21, 22, 24), the ADA effect was independent of its enzymatic activity, since a similar effect of wild-type ADA was observed using ADA inhibited with HgCl_2 , as described in Materials and Methods (Table 4). In contrast, the effect of wild-type ADA on $A_1\text{R}$ and $A_{2A}\text{R}$ was completely blocked when the enzyme was inhibited by preincubation (30 min) with 10 nM of the transition-state irreversible inhibitor deoxycoformycin (Table 4). Since deoxycoformycin stabilizes the closed form of the enzyme (54), the results indicated that the closed form is not able to induce the AR modulation.

To analyze the effect of ADA containing mutations within the α -1 helix, alanine substitutions for L58, D60, F61, L62, K64, F65, D66, and M69 (stretch L58-I72; Fig. 1A, violet) were performed (see Fig. 4E), tested on agonist binding to $A_1\text{R}$ and $A_{2A}\text{R}$ and compared with that of ADA wild type. From the ADA dose-response curves shown in Fig. 4, the EC_{50} and maximum increase of binding values were calculated and appear in Table 4. Whereas mutation of D66 did not lead to any significant differential effect, the other mutants were less efficient than wild-type ADA in enhancing the agonist binding to one or both receptors. Whereas

TABLE 2. Specific activity of wild-type and ADA mutants

Enzyme	Specific activity ($\mu\text{mol min}^{-1} \text{mg}^{-1}$)
Wild type	41.0
L58A	3.1
D60A	12.4
F61A	3.0
L62A	3.2
K64A	16.0
F65A	3.6
D66A	44.0
M69A	1.5
I115A	24.0
N118A	19.0
M155A	3.8
H157A	38.0
G184Q	10.5
D185A	6.9
L194A	48.0

Wild-type and mutant enzymes were partially purified as indicated in Materials and Methods. Specific activity was determined using the substrate concentration that gives V_{max} , and protein concentration was measured by the bicinchoninic acid method.

TABLE 3. Steady-state kinetic parameters for the wild-type and ADA mutants

Enzyme	k_{cat} (s^{-1})	K_m (μM)	k_{cat}/K_m ($M^{-1} s^{-1}$)	K_i (PR) (μM)
WT	190 ± 20	26 ± 3	7.3×10^6	13 ± 2
L58A	$9 \pm 1^{**}$	$183 \pm 12^{**}$	0.051×10^6	$>1000^{**}$
D60A	$87 \pm 9^{**}$	23 ± 3	3.8×10^6	11 ± 3
F61A	$13 \pm 2^{**}$	25 ± 2	0.52×10^6	20 ± 2
L62A	$19 \pm 2^{**}$	$250 \pm 30^{**}$	0.074×10^6	$>1000^{**}$
K64A	$92 \pm 8^{**}$	40 ± 6	2.3×10^6	32 ± 3
F65A	$80 \pm 10^{**}$	$200 \pm 17^{**}$	0.4×10^6	$>1000^{**}$
D66A	176 ± 19	33 ± 4	5.3×10^6	26 ± 2
M69A	$10 \pm 1^{**}$	25 ± 2	0.4×10^6	11 ± 2
I115A	$140 \pm 12^*$	28 ± 3	5.0×10^6	15 ± 3
N118A	$100 \pm 12^{**}$	35 ± 2	2.86×10^6	25 ± 3
M155A	$63 \pm 5^{**}$	$100 \pm 8^{**}$	0.63×10^6	$130 \pm 8^{**}$
H157A	170 ± 20	40 ± 6	4.25×10^6	$51 \pm 4^{**}$
G184Q	$115 \pm 10^{**}$	$78 \pm 4^{**}$	1.47×10^6	$120 \pm 10^{**}$
D185A	$80 \pm 6^{**}$	50 ± 3	1.6×10^6	$118 \pm 8^{**}$
L194A	173 ± 15	25 ± 2	6.9×10^6	15 ± 2

Steady state kinetic measurements were performed as indicated in Materials and Methods; values are means \pm SE of 3 separate experiments. Statistical differences with regard to control (wild-type ADA) were evaluated using 1-way ANOVA followed by a Dunnett's multiple comparison *post hoc* test. PR, purine riboside. * $P < 0.05$, ** $P < 0.01$.

mutations of D60, F61, K64, and F65 moderately affected the EC_{50} value or the maximum binding enhancement or both, mutation of M69 resulted in a lack of effect on $A_{2A}R$ binding paralleled with a 42-fold

increase in the EC_{50} value on the effect on A_1R binding. Finally, mutations of L58 and L62 were unable to significantly affect agonist binding to A_1R or to $A_{2A}R$ at concentrations < 1000 ng/ml. These results indicate

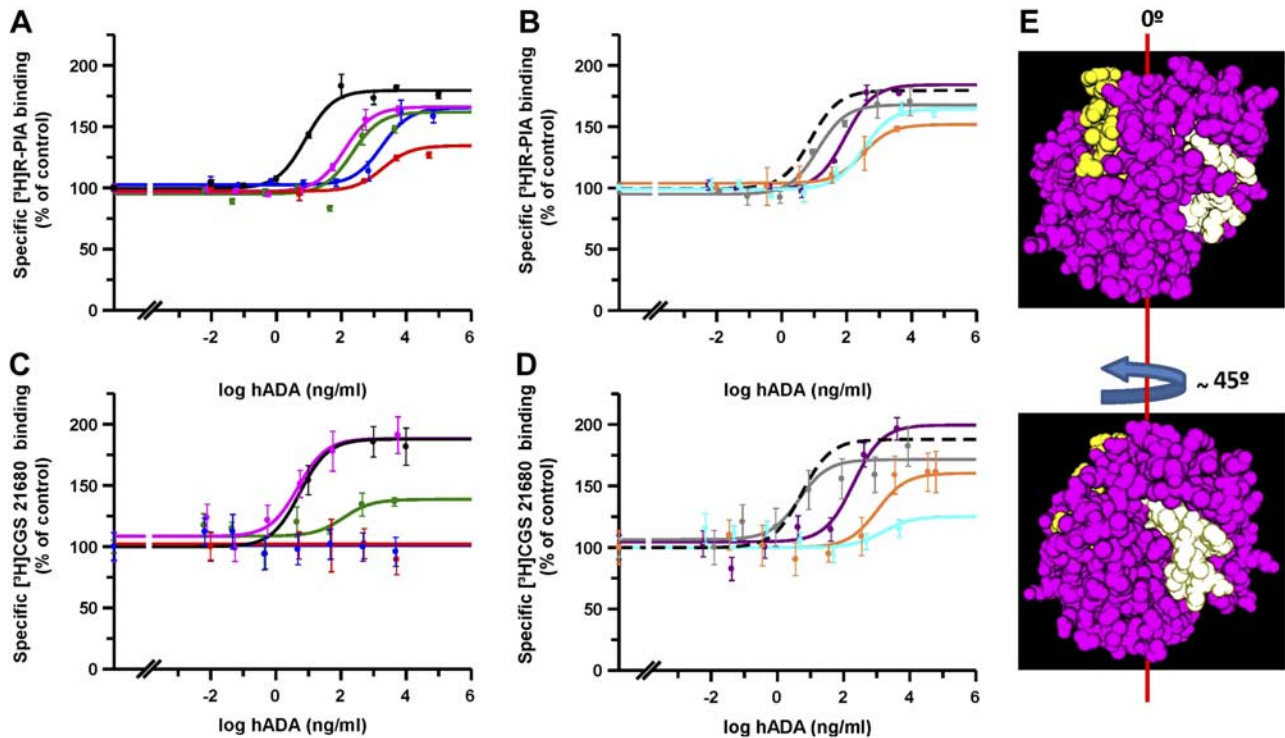


Figure 4. Effect of ADA helix α -1 mutations on agonist binding to A_1R and $A_{2A}R$. Binding of 0.5 nM [3H] (R)-PIA (A, B) and 20 nM [3H]CGS21680 (C, D) to brain striatal membranes (0.3 mg of protein/ml) was performed as described in Materials and Methods, in the absence or in the presence of increasing concentrations of ADA mutants. A, C) Dose-response curves corresponding to the mutants L58A (blue), D60A (green), F61A (magenta), and L62A (red). B, D) Dose-response curves corresponding to the mutants K64A (dark magenta), F65A (orange), D66A (gray), and M69A (cyan). Human ADA wild type is represented in black (continuous or dotted curve). Data are means \pm SE from a representative experiment ($n=3$) performed in triplicates. E) Surface representations of human ADA; helix α -1 (L58-I72) is shown in white, and helix α -2 (CD26 binding site, P126-D143) is in yellow. ADA (MMDDBID:75950) was drawn with Cn3D4.1 program (<http://www.ncbi.nlm.nih.gov>).

TABLE 4. Effect of wild-type and mutant ADA on the agonist binding to A₁R and A_{2A}R

Enzyme	A ₁ R		A _{2A} R	
	Δ[³ H](R)PIA binding (%)	EC ₅₀ (ng/ml)	Δ[³ H]CGS21680 binding (%)	EC ₅₀ (ng/ml)
WT	84 ± 6	8 ± 2	88 ± 10	7 ± 3
WT+HgCl ₂	86 ± 4	10 ± 3	80 ± 5	9 ± 3
WT+ DC	0**	>1500**	0**	>1500**
L58A	62 ± 5	>1500**	0**	>1500**
D60A	54 ± 3*	250 ± 30**	30 ± 7**	120 ± 10**
F61A	65 ± 8	130 ± 20**	90 ± 10	12 ± 4
L62A	34 ± 7**	>1500**	0**	>1500**
K64A	85 ± 7	90 ± 10*	95 ± 8	200 ± 4**
F65A	48 ± 9**	310 ± 40**	50 ± 10*	970 ± 120**
D66A	73 ± 6	13 ± 2	65 ± 10	4 ± 2
M69A	66 ± 4	330 ± 30**	25 ± 6**	>1500**
I115A	60 ± 10	10 ± 3	84 ± 8	5 ± 2
N118A	88 ± 8	10 ± 4	80 ± 8	5 ± 2
M155A	95 ± 10	120 ± 20**	92 ± 7	210 ± 60**
H157A	86 ± 5	7 ± 4	71 ± 9	11 ± 4
G184Q	89 ± 7	44 ± 7*	75 ± 8	24 ± 4
D185A	70 ± 8	112 ± 10**	40 ± 10**	>1500**
L194A	87 ± 6	12 ± 4	81 ± 10	9 ± 6
S03834	0**	>1500**	0**	>1500**

EC₅₀ value is the amount of wild type or mutant ADA that is able to produce the 50% of the maximum increase in 0.5 nM [³H] (R)-PIA binding to A₁R (Δ[³H](R)PIA binding) or 20 nM of [³H]CGS21680 binding to A_{2A}R (Δ[³H]CGS21680 binding). Values are means ± SE of 3 separate experiments. Statistical differences with regard to control (wild-type ADA) were evaluated using 1-way ANOVA followed by a Dunnett's multiple comparison *post hoc* test. DC, deoxycoformycin. **P* < 0.05, ***P* < 0.01.

that α-1 helix and its residues 58 and 62 are important for the ADA effect on A₁R and A_{2A}R and that M69 is affecting more the binding to A_{2A}R than to A₁R.

The effect of mutations in stretches 2 and 3, which are loops located near the α-1 helix in the tertiary structure of the enzyme (Fig. 5C, D), were tested as well. These stretches contain residues P114-N118 and M155-Q158 (see Fig. 2). The ADA dose-response effect on agonist binding to A₁R and A_{2A}R were determined using the same protocol described above. From these curves (Fig. 5), the values of EC₅₀ and maximum binding increase were calculated and appear in Table 4. Mutations of I115, N118, and H157 did not produce any significant change in the EC₅₀ values nor in the maximum effect when compared to the effect of wild-type ADA on both A₁R and A_{2A}R. Despite the finding that mutation of M155 moderately increased the EC₅₀ values without significantly affecting the maximum effect, these results suggest that these regions in the enzyme are not very important for the ADA-AR interaction. The moderate effect of the M155A mutant may be due to a structural alteration transmitted to the tertiary structure of the protein, affecting the conformation of the α-1 helix.

Finally, we tested the effect of mutations in stretch 4, the loop containing the residues A183-I188 (Fig. 1A, orange). This portion is also relatively close to the L58-I72 α-1 helix in the tertiary structure of the enzyme (Fig. 6C, D) and acts with the α-1 helix as a structural gate to close the catalytic pocket after substrate binding (40). The ADA dose-response effect on agonist binding

to A₁R and A_{2A}R was determined using the same protocol described above. From these curves (Fig. 6), the values of EC₅₀ and maximum binding increase were calculated and appear in Table 4. The G184Q and D185A mutants produced moderate and strong increase in the EC₅₀ values, respectively, without significant (G184Q) or moderate (D185A) changes in the maximum effect compared to wild-type ADA. These results suggest that this loop is important for ADA-induced modulation of the ARs. As a control, we tested the effect of alanine substitution for L194, since this residue in ADA does not seem to be related to stretches 1 and 4 (see Figs. 2 and 6D). From the dose-response curve (Fig. 6), the effect of such a mutant on both EC₅₀ and maximum binding was determined (Table 4) and was similar to those exerted by wild-type ADA (Table 4). As a further negative control, we used purified preparations of nontransformed *E. coli* SΦ 3834 extracts that do not contain any significant ADA. The dose-response curve using these preparations appears in Fig. 6 and indicates that *E. coli* SΦ 3834 preparations devoid of endogenous or recombinant ADA did not show any effect on agonist binding to A₁R or A_{2A}R (Table 4).

DISCUSSION

Many proteins are known to undergo big conformational changes on interacting with substrates, ligands, or other macromolecules. In the case of ADA, it has been observed that this enzyme has two distinct confor-

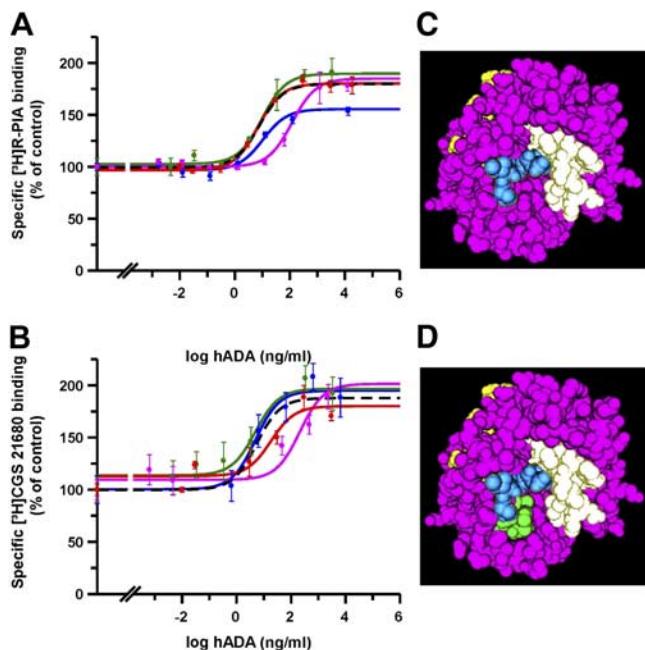


Figure 5. Effect of ADA mutations on 114-118 and 155-158 loops on agonists binding to A_1R and $A_{2A}R$. *A, B*) Binding of 0.5 nM [3H] (R)-PIA (*A*) and 20 nM [3H]CGS21680 (*B*) to brain striatal membranes (0.3 mg of protein/ml) was performed as described in Materials and Methods, in the absence or in the presence of increasing concentrations of ADA mutants. Dose-response curves correspond to the mutants I115A (blue), N118A (green), M155A (magenta), and H157A (red); human ADA wild type is represented in black (dotted curves). Data are means \pm SE from a representative experiment ($n=3$) performed in triplicates. *C, D*) Surface representations of human ADA; helix α -1 (L58-I72) is shown in white, helix α -2 (CD26 binding site, P126-D143) is in yellow, P114-N118 residues are in blue, and M155-G158 residues are in green (*D*). ADA (MMDBID:75950) was drawn with Cn3D4.1 program (<http://www.ncbi.nlm.nih.gov>).

mations, named the open form and the closed form (40, 54–56). The enzyme holds an α/β -barrel architecture and a TIM-barrel topology with a deep active site pocket and an essential tightly bound Zn^{2+} ion. Controlling access to the active site pocket is a structural gate consisting of an α helix (T57-A73) and the peptide backbone of a β strand (L182-D185). In the absence of substrate, the structural gate is open, and in the presence of substrate or inhibitors, such as deoxycoformycin or purine riboside, a conformational change can be detected, and the active site is in the closed form (39, 40, 54, 56–58), yet still largely solvent accessible in the closed mammalian ADA structures (59). Here we demonstrated that mutations of hydrophobic residues L58 and L62 on the structural gate α -1 helix results in a 2-order-of-magnitude decrease of the catalytic efficiency by decreasing both the substrate affinity and the maximum velocity. These results suggest that hydrophobicity may help to maintain the affinity for adenosine and control catalysis.

ADA is able to modulate the ligand binding to ARs. Docking simulations predicted that the two amino acid stretches that participate in the structural gate of the

active site pocket (Fig. 1A, violet and orange) participate in the interface between the agonist-bound form of $A_{2A}R$ and ADA. In line with docking predictions, alanine scanning mutagenesis demonstrated that these amino acid stretches play a central role in ADA-induced modulation of agonist binding to both the A_1R and $A_{2A}R$ subtypes. If the interacting portion between ADA and ARs is the structural gate, the region controlling open and closed forms, it seems reasonable to postulate that the open and closed forms of the enzyme may not interact equally with A_1R or $A_{2A}R$. In line with this hypothesis, the open forms of ADA gave better docking scores than the closed one. We observed that wild-type ADA is able to increase ligand binding to ARs in brain striatal membranes in the absence of the endogenous substrate adenosine. Since ADA is in the open form under these conditions (39, 40, 56), it appears that it is the open form that is able to bind to A_1R and $A_{2A}R$. This hypothesis is strengthened by the observation that in the presence of deoxycoformycin, a transition-state inhibitor of ADA that stabilizes the closed form (54), the effect of ADA on agonist binding to A_1R and $A_{2A}R$ is blocked (Table 4), in agreement with our previously

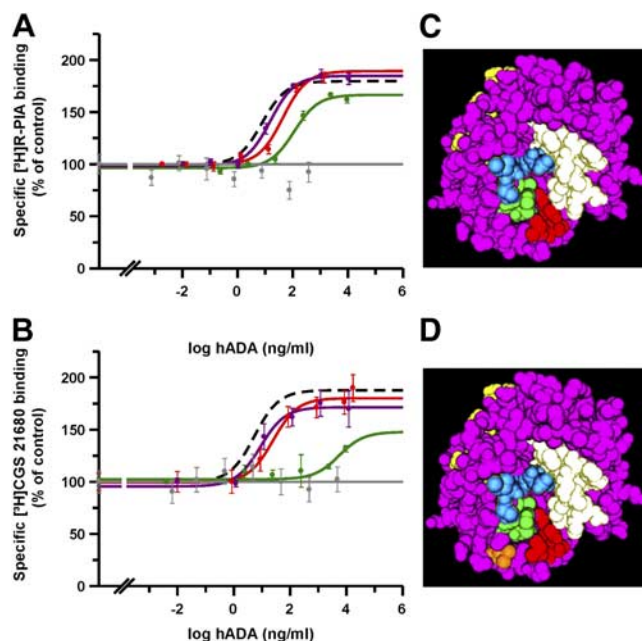


Figure 6. Effect of ADA mutation on 183-188 loop on agonists binding to A_1R and $A_{2A}R$. *A, B*) Binding of 0.5 nM [3H] (R)-PIA (*A*) and 20 nM [3H]CGS21680 (*B*) to brain striatal membranes (0.3 mg of protein/ml) was performed as described in Materials and Methods, in the absence or in the presence of increasing concentrations of ADA mutants. Dose-response curves correspond to the mutants G184G (red), D185A (green), L194A (dark magenta), or *E. coli* S Φ 3838 extracts not expressing ADA (gray); human ADA wild type is represented in black (dotted curves). Data are means \pm SE from a representative experiment ($n=3$) performed in triplicates. *C, D*) Surface representations of human ADA; helix α -1 (L58-I72) is shown in white, helix α -2 (CD26 binding site, P126-D143) is in yellow, P114-N118 residues are in blue, M155-G158 residues are in green, A183-I188 residues are in red, and L194 is in orange (*D*). ADA (MMDBID:75950) was drawn with Cn3D4.1 program (<http://www.ncbi.nlm.nih.gov>).

published results (27). Note that the enzymatic activity of ADA is not required to produce an increase in the agonist binding to A₁R and A_{2A}R, because Hg²⁺-inhibited ADA is able to enhance agonist binding to ARs. These results imply that Hg²⁺ binding to the enzyme gives rise to an inhibited open form of the enzyme.

The predicted complex between ADA and A_{2A}R is compatible with a supramolecular assembly in which ADA bridges A_{2A}R and CD26 (Fig. 1 C, D). This is in line with the notion that the interaction of ADA with ARs has an important role in the immunological synapse. In the immunosynapse, by interacting simultaneously with CD26 (on the surface of CD4⁺ T cells) and the AR (on the cell surface of dendritic cells), ADA triggers a costimulatory signal for human T cells that is critical in potentiating T-cell proliferation and activation (8, 10, 11). The intercellular interaction made by ARs, ADA, and CD26 increases the power of the effector phase of CD4⁺ T-cell responses and induces generation of memory and regulatory T cells (60). Thus, our results support the role of ADA as a bridge between cells expressing ARs and cells expressing CD26.

In the neurological synapse, adenosine acts as a potent neuromodulator by binding to ARs. One important effect of ADA in this process is to degrade adenosine in order to finish the receptor signaling. For many years, it had been assumed that this was the only role of ADA in ligand binding to ARs. Because of this, ADA is usually added to *in vitro* ligand binding experiments to avoid endogenous adenosine competition with AR ligands for the binding site. The first evidence that ADA also plays an enzyme-independent role on ARs came from the demonstration that ADA is able to bind A₁R, A_{2B}R, and A_{2A}R (20–26). This molecular interaction leads to a significant increase in the affinity of receptors for the agonist (21, 26). This allosteric effect was demonstrated to be independent of the enzymatic activity, because it happens with exhaustively washed membranes devoid of detectable adenosine or with inactivated ADA by pretreatment with Hg²⁺ ions (21, 24). Thus, the ecto-ADA can perform two roles. First, when the adenosine concentration is high, through its enzymatic activity, ADA reduces the available adenosine levels; thus, there is less stimulation of ARs, preventing the receptor desensitization. Second, independent from this enzymatic activity, by interacting with receptors, ADA can act as an allosteric modulator of ARs, increasing the adenosine binding at low adenosine concentrations (21, 24, 25). A new strategy to modulate the activity of GPCRs is to find allosteric modulators that are ligands able to bind to an allosteric site and increase or decrease the ligand binding to the receptor orthosteric site. By this definition, ADA is an allosteric ligand of A₁R and A_{2A}R that positively modulates the agonist binding to the orthosteric site. The allosteric modulators known so far for ARs are small organic compounds. One exception is a recently described antibody fragment that prevents agonist but not antagonist binding to A_{2A}R. Although this antibody fragment provides insights into the mechanisms of allosteric modulation

of GPCRs, the therapeutic implications are slight, since they recognize the intracellular portion of A_{2A}R (61). The allosteric interaction described here suggests a novel strategy to modulate GPCR function, which relies on small molecules acting on extracellular proteins bound to the GPCR, *i.e.*, drugs acting on ADA, which allosterically modulates the AR properties. The interest in allosteric modulators is more relevant in the case of neurotransmitter receptor targets due to the fact that synaptic neurotransmission occurs in extremely complex circuits implicated in many neurological functions. The presence of ADA bound to the cell surface of neurons has been demonstrated (62), thus reinforcing the concept that this allosteric effect of ADA is likely to occur *in vivo*. More than 70 ADA mutations have been found in patients with SCID (5), and it will be interesting to know whether some of these mutations interfere with the interaction of ADA with ARs. In this respect, it would be worth investigating whether the modulatory role of ADA on AR function is perturbed due to mutation, which would imply neurological alterations in addition to immunological alterations as associated with selected ADA SCID-causing mutations. Thus, unveiling the ADA portions involved in the interaction with the ARs may help discriminate ADA SCID mutations characterized by neurological effects from those having only immunological effects.

In summary, the results of this study led to several major conclusions on the interaction of ADA with A₁R and A_{2A}R. First, we described an A₁R and A_{2A}R allosteric modulation by an extracellular protein. In this interaction, the ADA α -1 helix containing residues L58-I72 and the loop containing residues A183-I188 are important to maintain both the catalytic efficiency of ADA and its functional interaction with both ARs. Second, the predicted interaction mode between ADA and A_{2A}R is such that a continuous channel connects the adenosine binding site on the A_{2A}R and the catalytic pocket of ADA. Third, the predicted architecture of the ADA-A_{2A}R complex is compatible with a supramolecular assembly, in which ADA acts as a bridge between A_{2A}R and CD26. This is consistent with the hypothesis that ADA may bridge dendritic cells and lymphocytes in the immunosynapse triggering costimulation. Finally, we suggest that it is the open form of ADA but not the closed one that is able to functionally interact with A₁R and A_{2A}R. In addition, our results suggest the role of ADA hydrophobic residues in maintaining the adenosine affinity and controlling the catalysis. EJ

The authors acknowledge the technical help obtained from Jasmina Jiménez (Laboratory of Molecular Neurobiology, University of Barcelona) and Francesco Raimondi (University of Modena and Reggio Emilia). This study was supported by grants from the Spanish Ministerio de Ciencia y Tecnología (SAF2010-18472, SAF2011-23813 and SAF2008-3229-E/ within the frame of the Era-NET Neuron program), grant for collaborative projects PI2011/02-7 from the Centro de Investigación Biomédica en Red sobre Enfermedades Neurodegenerativas (CIBERNED), and by FIPSE (a non-

profit foundation including the Spanish Ministry of Health, Abbott Laboratories, Boehringer Ingelheim, Bristol Myers Squibb, GlaxoSmithKline, Merck Sharp and Dohme, and Roche) grant 36750/08. This study was also supported by Telethon-Italy grant S00068TELU (to F.F.). P.J.M. is a Ramón y Cajal Fellow.

REFERENCES

- Cristalli, G., Costanzi, S., Lambertucci, C., Lupidi, G., Vittori, S., Volpini, R., and Camaioni, E. (2001) Adenosine deaminase: functional implications and different classes of inhibitors. *Med. Res. Rev.* **21**, 105–128
- Petersen, M. B., Tranebjaerg, L., Tommerup, N., Nygaard, P., and Edwards, H. (1987) New assignment of the adenosine deaminase gene locus to chromosome 20q13 X 11 by study of a patient with interstitial deletion 20q. *J. Med. Genet.* **24**, 93–96
- Arredondo-Vega, F. X., Santisteban, I., Daniels, S., Toutain, S., and Hershfield, M. S. (1998) Adenosine deaminase deficiency: genotype-phenotype correlations based on expressed activity of 29 mutant alleles. *Am. J. Hum. Genet.* **63**, 1049–1059
- Resta, R., and Thompson, L. F. (1997) SCID: the role of adenosine deaminase deficiency. *Immunol. Today* **18**, 371–374
- Hershfield, M. S. (2003) Genotype is an important determinant of phenotype in adenosine deaminase deficiency. *Curr. Opin. Immunol.* **15**, 571–577
- Kameoka, J., Tanaka, T., Nojima, Y., Schlossman, S. F., and Morimoto, C. (1993) Direct association of adenosine deaminase with a T cell activation antigen, CD26. *Science* **261**, 466–469
- Franco, R., Valenzuela, A., Lluís, C., and Blanco, J. (1998) Enzymatic and extraenzymatic role of ecto-adenosine deaminase in lymphocytes. *Immunol. Rev.* **161**, 27–42
- Pacheco, R., Martínez-Navio, J. M., Lejeune, M., Climent, N., Oliva, H., Gatell, J. M., Gallart, T., Mallol, J., Lluís, C., and Franco, R. (2005) CD26, adenosine deaminase, and adenosine receptors mediate costimulatory signals in the immunological synapse. *Proc. Natl. Acad. Sci. U. S. A.* **102**, 9583–9588
- Engel, M., Hoffmann, T., Wagner, L., Wermann, M., Heiser, U., Kiefersauer, R., Huber, R., Bode, W., Demuth, H. U., and Brandstetter, H. (2003) The crystal structure of dipeptidyl peptidase IV (CD26) reveals its functional regulation and enzymatic mechanism. *Proc. Natl. Acad. Sci. U. S. A.* **100**, 5063–5068
- Dong, R. P., and Morimoto, C. (1996) Role of CD26 for CD4 memory T cell function and activation. *Hum. Cell* **9**, 153–162
- Dong, R. P., Tachibana, K., Hegen, M., Munakata, Y., Cho, D., Schlossman, S. F., and Morimoto, C. (1997) Determination of adenosine deaminase binding domain on CD26 and its immunoregulatory effect on T cell activation. *J. Immunol.* **159**, 6070–6076
- Havre, P. A., Abe, M., Urasaki, Y., Ohnuma, K., Morimoto, C., and Dang, N. H. (2008) The role of CD26/dipeptidyl peptidase IV in cancer. *Front. Biosci.* **13**, 1634–1645
- Kajiyama, H., Kikkawa, F., Khin, E., Shibata, K., Ino, K., and Mizutani, S. (2003) Dipeptidyl peptidase IV overexpression induces up-regulation of E-cadherin and tissue inhibitors of matrix metalloproteinases, resulting in decreased invasive potential in ovarian carcinoma cells. *Cancer Res.* **63**, 2278–2283
- Kikkawa, F., Kajiyama, H., Ino, K., Shibata, K., and Mizutani, S. (2003) Increased adhesion potency of ovarian carcinoma cells to mesothelial cells by overexpression of dipeptidyl peptidase IV. *Int. J. Cancer* **105**, 779–783
- Wesley, U. V., Albino, A. P., Tiwari, S., and Houghton, A. N. (1999) A role for dipeptidyl peptidase IV in suppressing the malignant phenotype of melanocytic cells. *J. Exp. Med.* **190**, 311–322
- Kameoka, J., Ichinohasama, R., Inoue, H., Yamamoto, J., Yokoyama, H., Tomiya, Y., Yamada, M., Ishizawa, K., Harigae, H., Sawai, T., and Sasaki, T. (2006) CD26, together with cell surface adenosine deaminase, is selectively expressed on ALK-positive, but not on ALK-negative, anaplastic large cell lymphoma and Hodgkin's lymphoma. *Leuk. Lymphoma* **47**, 2181–2188
- Richard, E., Arredondo-Vega, F. X., Santisteban, I., Kelly, S. J., Patel, D. D., and Hershfield, M. S. (2000) The binding site of human adenosine deaminase for CD26/Dipeptidyl peptidase IV: the Arg142Gln mutation impairs binding to cd26 but does not cause immune deficiency. *J. Exp. Med.* **192**, 1223–1236
- Richard, E., Alam, S. M., Arredondo-Vega, F. X., Patel, D. D., and Hershfield, M. S. (2002) Clustered charged amino acids of human adenosine deaminase comprise a functional epitope for binding the adenosine deaminase complexing protein CD26/dipeptidyl peptidase IV. *J. Biol. Chem.* **277**, 19720–19726
- Weihofen, W. A., Liu, J., Reutter, W., Saenger, W., and Fan, H. (2004) Crystal structure of CD26/dipeptidyl-peptidase IV in complex with adenosine deaminase reveals a highly amphiphilic interface. *J. Biol. Chem.* **279**, 43330–43335
- Ciruela, F., Saura, C., Canela, E. I., Mallol, J., Lluís, C., and Franco, R. (1996) Adenosine deaminase affects ligand-induced signalling by interacting with cell surface adenosine receptors. *FEBS Lett.* **380**, 219–223
- Gracia, E., Cortés, A., Meana, J. J., García-Sevilla, J., Hershfield, M. S., Canela, E. I., Mallol, J., Lluís, C., Franco, R., and Casadó, V. (2008) Human adenosine deaminase as an allosteric modulator of human A(1) adenosine receptor: abolishment of negative cooperativity for [H](R)-pia binding to the caudate nucleus. *J. Neurochem.* **107**, 161–170
- Saura, C., Ciruela, F., Casadó, V., Canela, E. I., Mallol, J., Lluís, C., and Franco, R. (1996) Adenosine deaminase interacts with A1 adenosine receptors in pig brain cortical membranes. *J. Neurochem.* **66**, 1675–1682
- Sun, W. C., Cao, Y., Jin, L., Wang, L. Z., Meng, F., and Zhu, X. Z. (2005) Modulating effect of adenosine deaminase on function of adenosine A1 receptors. *Acta Pharmacol. Sin.* **26**, 160–165
- Gracia, E., Pérez-Capote, K., Moreno, E., Bakesova, J., Mallol, J., Lluís, C., Franco, R., Cortés, A., Casadó, V., and Canela, E. I. (2011) A2A adenosine receptor ligand binding and signaling is allosterically modulated by adenosine deaminase. *Biochem. J.* **435**, 701–709
- Herrera, C., Casadó, V., Ciruela, F., Schofield, P., Mallol, J., Lluís, C., and Franco, R. (2001) Adenosine A2B receptors behave as an alternative anchoring protein for cell surface adenosine deaminase in lymphocytes and cultured cells. *Mol. Pharmacol.* **59**, 127–134
- Saura, C. A., Mallol, J., Canela, E. I., Lluís, C., and Franco, R. (1998) Adenosine deaminase and A1 adenosine receptors internalize together following agonist-induced receptor desensitization. *J. Biol. Chem.* **273**, 17610–17617
- Torvinen, M., Ginés, S., Hillion, J., Latini, S., Canals, M., Ciruela, F., Bordoni, F., Staines, W., Pedata, F., Agnati, L. F., Lluís, C., Franco, R., Ferré, S., and Fuxe, K. (2002) Interactions among adenosine deaminase, adenosine A(1) receptors and dopamine D(1) receptors in stably cotransfected fibroblast cells and neurons. *Neuroscience* **113**, 709–719
- Climent, N., Martínez-Navio, J. M., Gil, C., Garcia, F., Rovira, C., Hurtado, C., Miralles, L., Gatell, J. M., Gallart, T., Mallol, J., Lluís, C., and Franco, R. (2009) Adenosine deaminase enhances T-cell response elicited by dendritic cells loaded with inactivated HIV. *Immunol. Cell. Biol.* **87**, 634–639
- Martínez-Navio, J. M., Climent, N., Pacheco, R., Garcia, F., Plana, M., Nomdedeu, M., Oliva, H., Rovira, C., Miralles, L., Gatell, J. M., Gallart, T., Mallol, J., Lluís, C., and Franco, R. (2009) Immunological dysfunction in HIV-1-infected individuals caused by impairment of adenosine deaminase-induced costimulation of T-cell activation. *Immunology* **128**, 393–404
- Chen, R., Li, L., and Weng, Z. (2003) ZDOCK: an initial-stage protein-docking algorithm. *Proteins* **52**, 80–87
- Canals, M., Marcellino, D., Fanelli, F., Ciruela, F., De Benedetti, P., Goldberg, S. R., Neve, K., Fuxe, K., Agnati, L. F., Woods, A. S., Ferré, S., Lluís, C., Bouvier, M., and Franco, R. (2003) Adenosine A2A-dopamine D2 receptor-receptor heteromerization: qualitative and quantitative assessment by fluorescence and bioluminescence energy transfer. *J. Biol. Chem.* **278**, 46741–46749
- Casciari, D., Dell'Orco, D., and Fanelli, F. (2008) Homodimerization of neurotensin 1 receptor involves helices 1, 2, and 4: insights from quaternary structure predictions and dimerization free energy estimations. *J. Chem. Inf. Model.* **48**, 1669–1678
- Casciari, D., Seeber, M., and Fanelli, F. (2006) Quaternary structure predictions of transmembrane proteins starting from

- the monomer: a docking-based approach. *BMC Bioinformatics* **7**, 340
34. Fanelli, F. (2007) Dimerization of the lutropin receptor: insights from computational modeling. *Mol. Cell. Endocrinol.* 260–262, 59–64
 35. Fanelli, F., Mauri, M., Capra, V., Raimondi, F., Guzzi, F., Ambrosio, M., Rovati, G. E., and Parenti, M. (2011) Light on the structure of thromboxane A2 receptor heterodimers. *Cell. Mol. Life Sci.* **68**, 3109–3120
 36. Fanelli, F., and Felline, A. (2011) Dimerization and ligand binding affect the structure network of A(2A) adenosine receptor. *Biochim. Biophys. Acta* **1808**, 1256–1266
 37. Heyer, L. J., Kruglyak, S., Yooseph, S. (1999) Exploring expression data: identification and analysis of coexpressed genes. *Genome Res.* **9**, 1106–1115
 38. Lebon, G., Warne, T., Edwards, P. C., Bennett, K., Langmead, C. J., Leslie, A. G., and Tate, C. G. (2011) Agonist-bound adenosine A2A receptor structures reveal common features of GPCR activation. *Nature* **474**, 521–525
 39. Kinoshita, T., Nishio, N., Nakanishi, I., Sato, A., and Fujii, T. (2003) Structure of bovine adenosine deaminase complexed with 6-hydroxy-1,6-dihydropurine riboside. *Acta Crystallogr. A* **59**, 299–303
 40. Kinoshita, T., Nakanishi, I., Terasaka, T., Kuno, M., Seki, N., Warizaya, M., Matsumura, H., Inoue, T., Takano, K., Adachi, H., Mori, Y., and Fujii, T. (2005) Structural basis of compound recognition by adenosine deaminase. *Biochemistry* **44**, 10562–10569
 41. Cieplak, P., and Kollman, P. A. (1996) A technique to study molecular recognition in drug design: preliminary application of free energy derivatives to inhibition of a malarial cysteine protease. *J. Mol. Recognit.* **9**, 103–112
 42. Lu, H., and Schulten, K. (1999) Steered molecular dynamics simulations of force-induced protein domain unfolding. *Proteins* **35**, 453–463
 43. Phillips, J. C., Braun, R., Wang, W., Gumbart, J., Tajkhorshid, E., Villa, E., Chipot, C., Skeel, R. D., Kale, L., and Schulten, K. (2005) Scalable molecular dynamics with NAMD. *J. Comput. Chem.* **26**, 1781–1802
 44. York, D. M., Wlodawer, A., Pedersen, L. G., and Darden, T. A. (1994) Atomic-level accuracy in simulations of large protein crystals. *Proc. Natl. Acad. Sci. U. S. A.* **91**, 8715–8718
 45. van Gunsteren, W. F., and Berendsen, H. J. (1987) Thermodynamic cycle integration by computer simulation as a tool for obtaining free energy differences in molecular chemistry. *J. Comput. Aided Mol. Des.* **1**, 171–176
 46. Chandler, D., Weeks, J. D., and Andersen, H. C. (1983) Van der Waals picture of liquids, solids, and phase transformations. *Science* **220**, 787–794
 47. Rueda, M., Ferrer-Costa, C., Meyer, T., Perez, A., Camps, J., Hospital, A., Gelpí, J.L., and Orozco, M. (2007) A consensus view of protein dynamics. *Proc. Natl. Acad. Sci. U. S. A.* **104**, 796–801
 48. Meyer, T., D'Abramo, M., Hospital, A., Rueda, M., Ferrer-Costa, C., Pérez, A., Carrillo, O., Camps, J., Fenollosa, C., Repchevsky, D., Gelpí, J.L., and Orozco, M. (2010) MoDEL (Molecular Dynamics Extended Library): a database of atomistic molecular dynamics trajectories. *Structure* **18**, 1399–1409
 49. Fernández-Recio, J., Totrov, M., Skorodumov, C., and Abagyan, R. (2005) Optimal docking area: a new method for predicting protein-protein interaction sites. *Proteins* **58**, 134–143
 50. Cheng, T. M., Blundell, T. L., and Fernández-Recio, J. (2007) pyDock: electrostatics and desolvation for effective scoring of rigid-body protein-protein docking. *Proteins* **68**, 503–511
 51. Chang, Z. Y., Nygaard, P., Chinault, A. C., Kellems, R. E. (1991) Deduced amino acid sequence of Escherichia coli adenosine deaminase reveals evolutionarily conserved amino acid residues: implications for catalytic function. *Biochemistry* **30**, 2273–2280
 52. Smith, P. K., Krohn, R. I., Hermanson, G. T., Mallia, A. K., Gartner, F. H., Provenzano, M. D., Fujimoto, E. K., Goeke, N. M., Olson, B. J., and Klenk, D. C. (1985) Measurement of protein using bicinchoninic acid. *Anal. Biochem.* **150**, 76–85
 53. Casadó, V., Cantí, C., Mallol, J., Canela, E. I., Lluís, C., and Franco, R. (1990) Solubilization of A1 adenosine receptor from pig brain: characterization and evidence of the role of the cell membrane on the coexistence of high- and low-affinity states. *J. Neurosci. Res.* **26**, 461–473
 54. Wang, Z., and Quijochó, F. A. (1998) Complexes of adenosine deaminase with two potent inhibitors: X-ray structures in four independent molecules at pH of maximum activity. *Biochemistry* **37**, 8314–8324
 55. Wilson, D. K., and Quijochó, F. A. (1993) A pre-transition-state mimic of an enzyme: X-ray structure of adenosine deaminase with bound 1-deazaadenosine and zinc-activated water. *Biochemistry* **32**, 1689–1694
 56. Wilson, D. K., Rudolph, F. B., and Quijochó, F. A. (1991) Atomic structure of adenosine deaminase complexed with a transition-state analog: understanding catalysis and immunodeficiency mutations. *Science* **252**, 1278–1284
 57. Kinoshita, T., Tada, T., and Nakanishi, I. (2008) Conformational change of adenosine deaminase during ligand-exchange in a crystal. *Biochem. Biophys. Res. Commun.* **373**, 53–57
 58. Terasaka, T., Kinoshita, T., Kuno, M., and Nakanishi, I. (2004) A highly potent non-nucleoside adenosine deaminase inhibitor: efficient drug discovery by intentional lead hybridization. *J. Am. Chem. Soc.* **126**, 34–35
 59. Larson, E. T., Deng, W., Krumm, B. E., Napuli, A., Mueller, N., Van Voorhis, W. C., Buckner, F. S., Fan, E., Lauricella, A., DeTitta, G., Luft, J., Zucker, F., Hol, W. G., Verlinde, C. L., and Merritt, E. A. (2008) Structures of substrate- and inhibitor-bound adenosine deaminase from a human malaria parasite show a dramatic conformational change and shed light on drug selectivity. *J. Mol. Biol.* **381**, 975–988
 60. Martínez-Navío, J. M., Casanova, V., Pacheco, R., Naval-Macabuhay, I., Climent, N., García, F., Gatell, J. M., Mallol, J., Gallart, T., Lluís, C., and Franco, R. (2011) Adenosine deaminase potentiates the generation of effector, memory, and regulatory CD4+ T cells. *J. Leukoc. Biol.* **89**, 127–136
 61. Hino, T., Arakawa, T., Iwanari, H., Yurugi-Kobayashi, T., Ikeda-Suno, C., Nakada-Nakura, Y., Kusano-Arai, O., Weyand, S., Shimamura, T., Nomura, N., Cameron, A. D., Kobayashi, T., Hamakubo, T., Iwata, S., and Murata, T. (2012) G-protein-coupled receptor inactivation by an allosteric inverse-agonist antibody. *Nature* **482**, 237–240
 62. Ruíz, M. A., Escriche, M., Luís, C., Franco, R., Martín, M., Andrés, A., and Ros, M. (2000) Adenosine A(1) receptor in cultured neurons from rat cerebral cortex: colocalization with adenosine deaminase. *J. Neurochem.* **75**, 656–664
 63. Harris, R., Olson, A. J., and Goodsell, D. S. (2008) Automated prediction of ligand-binding sites in proteins. *Proteins* **70**, 1506–1517
 64. Frishman, D., and Argos, P. (1995) Knowledge-based protein secondary structure assignment. *Proteins* **23**, 566–579

Received for publication July 2, 2012.

Accepted for publication November 13, 2012.